Insights into hydrogen transport behavior on perovskite surfaces: Transition from the Grotthuss mechanism to the "vehicle" mechanism

Qian Li,[a] Qiang Yin,[a] Ya-Shan Zheng,[a] Zhi-Jun Sui,[a] Xing-Gui Zhou,[a] De Chen,[b] Yi-An Zhu[a],*

[a] United Chemical Reaction Engineering Research Institute (UNILAB), State Key Laboratory of Chemical Engineering, East China University of Science and Technology, Shanghai 200237, China.

[b] Department of Chemical Engineering, Norwegian University of Science and Technology, N-7491 Trondheim, Norway

[*] Author to whom correspondence should be addressed. E-mail: yanzhu@ecust.edu.cn.

ABSTRACT

Hydrogen transport on transition-metal oxides is a shared process in many important physical and chemical changes of interest. In this contribution, DFT+U calculations have been carried out to explore the mechanism for hydrogen migration on the defect-free and oxygen-deficient $LaMO_3(001)$ (M = Cr, Mn, and Fe) surfaces. Calculated results indicate that hydrogen is preferentially adsorbed at the oxygen sites on all the surfaces other than the defective $LaCrO_3(001)$, where the occupation of vacancies is energetically most favorable. The resultant O-H bonds would be weakened when oxygen vacancies are formed in their immediate vicinity, because the increased electron density on the remaining ions would limit the ability of O to withdraw electrons from H. On the defect-free $LaMO_3(001)$ hydrogen prefers to migrate along the [010] axis, during which the O-H bond is reoriented at the oxygen site for the hopping to proceed by the Grotthuss mechanism. In the presence of oxygen vacancies, the "vehicle" mechanism in which hydrogen hops together with the underlying oxygen would dominate on $LaMnO_3$ and $LaFeO_3$, whereas on the defective $LaCrO_3(001)$ the Grotthuss mechanism prevails. The linear scaling relations established show that the hydrogen and hydroxyl migration barriers decrease and increase, respectively, with increasing the strength of ionic bonding in perovskites, which provides a rational interpretation of the change in the preferred hydrogen migration mechanism.

KEYWORDS: Perovskite; Transport; Hydrogen; Grotthuss mechanism; "Vehicle" mechanism

INTRODUCTION

Surface protonics has recently attained considerable attention in the areas of catalysis and electrocatalysis[1-5]. In most of the related heterogeneous reactions, a shared process is the proton/hydrogen transport on metal oxides, and the rate for this process often determines the chemical reactivity of H-containing species and surfaces[6-7]. For instance, in catalytic steam reforming the proton conduction via adsorbed water was found to play an important role in methane activation on the Pd/CeO_2 catalyst surface at low temperature[3]. As another example, the temperature dependence of the reaction rate for methanol dissociation was ascribed to the varying migration ability of proton on the rutile TiO_2 catalyst, which significantly affects the possibility of reverse reactions and thus changes the amount of products[4]. In proton conducting fuel cells (PCFCs), perovskite-type transition-metal oxides have been reported to show high mobility of protonic defects and can therefore be used as proton-conducting electrolytes. Since the electrolyte surface is necessary to complete the electrical circuit of PCFCs, a full picture of how the perovskite materials behave therein can only be achieved through an understanding of the proton

migration behaviors in all the individual parts of the electrolytes, including grains, grain boundaries, and surfaces.

The proton/hydrogen transport in the bulk of transition-metal oxides has been the subject of many studies over the years and two distinctly different mechanisms have been proposed to account for the observed proton conductivity. One is the Grotthuss mechanism, which occurs mainly by rotational migration of a proton around an oxygen ion, followed by proton transfer toward a neighboring oxide ion, thereby consisting of a sequence of O-H$\cdots$O transfer and O-H bond reorientation[8-9]. In this mechanism, the reorientation step was generally believed to be fast with a low activation energy, suggesting that the proton transfer is rate limiting[10-12]. However, hydrogen bonding was found to play a major role in determining the proton/hydrogen transport kinetics. Infrared absorption spectroscopy studies of proton-conducting materials revealed a pronounced redshift in the O-H stretching band, which is characteristic of strongly hydrogen-bonded configurations[13]. It seems that the short and strong hydrogen bonds favor rapid proton transfer but are not beneficial to the O-H bond reorientation that requires breaking of hydrogen bonds[9], so possibly hindering the long-range proton migration by decreasing the reorientation rate. The other mechanism is along the "vehicle" pathway, in which proton is conducted by the migration of OH (OH^- and/or H_3O^+ in aqueous systems), with the oxygen in the hydroxyl ion functioning as the vehicle[14]. While this model is supported by the fact that the proton conductivity is strongly dependent on the oxygen vacancy concentration[15], it has difficulty in explaining the H/D isotope effect on the observed electrochemical

performance[16]. As a result, the proton diffusion pathway in bulk oxide continues to be controversial, although the Grotthuss mechanism is generally accepted to be dominant.

Compared to the many attempts that have been made to formulate the mechanism for the proton migration in the grains and across the grain boundaries of metal oxides, little theoretical effort has been devoted to understanding the proton/hydrogen conduction on the oxide surfaces. Kim et al[17-18] explored the proton migration along and across the energetically favorable BaO- and ZrO_2-terminated $BaZrO_3$(001) by performing density functional theory (DFT) calculations, claiming that proton can be readily conducted along the stoichiometric ZrO_2-terminated surface via proton transfer and rotation; that is, the proton surface migration follows the Grotthuss mechanism in the absence of surface oxygen vacancy. Kowalski et al.[19] and Yin et al.[20] studied the diffusion of H atoms from the fully hydroxylated surface into the bulk of the oxide and suggested that it is much more favorable for the H atoms to migrate into the bulk rather than desorbing from the surface. In their work, however, the possibility of the H migration on both the stoichiometric and the oxygen-deficient surfaces was disregarded.

La-based perovskites constitute one of the most important classes of ceramic materials, of which the $3d$-block transition-metal oxides are often applied as catalysts in many heterogeneous catalytic processes that involve hydrogen or proton, such as selective oxidation reactions[21] and reforming reactions for hydrogen and syngas production[22]. Since H would be tightly bound to surface O ions, the hydrogen mobility not only determines how frequently H atoms encounter one another to recombine to form H_2 molecules but also

affects the energetics of adsorption and activation of other reaction intermediates through adsorbate-adsorbate interaction. In this contribution, DFT+U calculations have been carried out to examine the proton migration mechanism on three representative $LaMO_3$ (M = Cr, Mn, and Fe) surfaces. The preferred adsorption sites and the adsorption energies of hydrogen on both defect-free and oxygen-deficient surfaces are first studied. Then, the climbing-image nudged elastic band (CI-NEB) method is used to calculate the hydrogen migration barriers for all the possible elementary steps and pathways by finding the minimum energy paths (MEPs). Next, the transition of the hydrogen transport pathway from the Grotthuss mechanism to the "vehicle" mechanism has been discussed. Finally, we conclude by identifying the key factor that determines the energy barriers for the hydrogen and hydroxyl ion migration on the perovskite surfaces.

COMPUTATIONAL DETAILS

All spin-polarized DFT calculations were carried out using the VASP code[23-25]. The Bayesian error estimation functional with van der Waals correlation (BEEF-vdW)[26] was used to treat the exchange and correlation of the Kohn-Sham theory, and the projector-augmented wave (PAW) method was applied to describe the interactions between ion cores and valence electrons[27]. By using the "hard" PAW potentials with valence configurations La ($5s^2\ 5p^6\ 6s^2\ 5d^1$), O_s ($2s^2\ 2p^4$), Cr_{pv} ($3p^6\ 3d^5\ 4s^1$), Mn_{pv} ($3p^6\ 3d^5\ 4s^2$), and Fe_{pv} ($3p^6\ 3d^6\ 4s^2$), a plane-wave energy cutoff of up to 600 eV was necessary to converge the total energy per atom to within 1 meV. Because standard exchange-correlation functionals

suffer from the "self-interaction error"[28], which is connected with the spurious interaction of an electron with itself and leads to excessive electron delocalization, an additional Hubbard-type term was applied in the simplified (rotationally invariant) DFT+U method[29-31]. The effective U (U_{eff}) values for the transition metals in $LaMO_3$ were obtained by fitting the calculated energetics of transition-metal oxide formation to available experimental data (U_{eff} = 2.5, 3.5, and 2.9 eV for Cr, Mn, and Fe, respectively[32]), in much the same way as that proposed by Wang et al.[33], Jain et al.[34], and Zeng et al. [35] (instead of making a correction to the oxygen binding energy, they took gas-phase H_2O and H_2 as the reference states to derive the thermodynamic quantities of transition-metal oxides, hydroxides, and oxyhydroxides). Electronic occupancies were determined according to the Gaussian scheme with an energy smearing of 0.1 eV. Since magnetic elements are involved in the systems, spin-polarized calculations were performed to obtain reasonably accurate structures and energetics, in which ferromagnetic ordering was adopted to approximate the paramagnetic state of the transition-metal oxides at relatively high temperatures[36].

It was reported that under mild conditions the $LaMO_3$ (M = Cr, Mn, and Fe) perovskites adopt an orthorhombic structure with the space group *Pbnm*. Before cleaving surface, the bulk structures of the stoichiometric perovskites were first optimized by using a quasi-Newton algorithm, with both lattice vectors and atomic coordinates allowed to relax. Then the equilibrium lattice constants obtained were kept fixed during the construction of surface models and the calculation of surface processes. The $LaMO_3(001)$ surface was represented as a eleven-layer slab with a $p(1 \times 1)$ cell, and a 12 Å vacuum spacing was

applied to separate two adjacent slabs in the direction perpendicular to the oxide surface. The bottom four layers of the slab were kept fixed at their crystal lattice positions while the adsorbate and the remainder of the slab were allowed to fully relax. For such a model, integration over the first Brillouin zone was performed using the Monkhorst-Pack[37] k-point sampling method, and a gamma-centered $4 \times 4 \times 1$ grid proves to be sufficient to converge the total energy per atom to less than 1 meV. As a first test of our methods, a $p(2 \times 2)$ supercell with the same MO_2 termination and a fifteen-layer slab have also been constructed to explore the energy dependence on the cell size and slab thickness, respectively. It is demonstrated that the use of the larger supercells can only change the hydrogen adsorption energy by less than 0.02 eV, suggesting that the $p(1 \times 1)$ cell can give a reasonably reliable description of the energetics of bond formation on the perovskite surfaces (The data are included in the Supporting Information).

The CI-NEB method[38-39], an improved version of the NEB method, was used to find the minimum energy path (MEP) for hydrogen migration elementary steps, where a certain number of images were first created between two energetically favorable stationary points and then optimized by using a force-based conjugate-gradient method. Both geometry optimization and transition-state search were considered to be converged when the forces on each atom were better than 0.03 eV/Å.

RESULTS AND DISCUSSION

Adsorption of hydrogen on LaMO₃ surfaces. The microstructure of perovskite AMO_3 can be well represented as a three-dimensional framework of corner-sharing MO_6

octahedra, where the A-site cations are centered in the cuboctahedral cavities of the MO_6 arrangement. Because of the size mismatch between the La and O ions as determined by the Goldschmidt tolerance factor, the MO_6 octahedra in the $LaMO_3$ (M= Cr, Mn, and Fe) tend to be tilted cooperatively to give an orthorhombic structure.

Unlike their counterparts in the bulk, the exposed O ions on the MO_2-terminated (001) surface are no longer equivalent and can be divided into two groups, which lie above and below the M cations and are denoted O_1 and O_2 (see Fig. 1a), respectively. Thus, there appear to be three possible hydrogen adsorption sites (i.e., the O_1, O_2, and M sites) on the $LaMO_3$(001) surface, although upon geometry optimization the two groups of O ions move either downward or upward and are eventually located in nearly the same plane as the M cation.
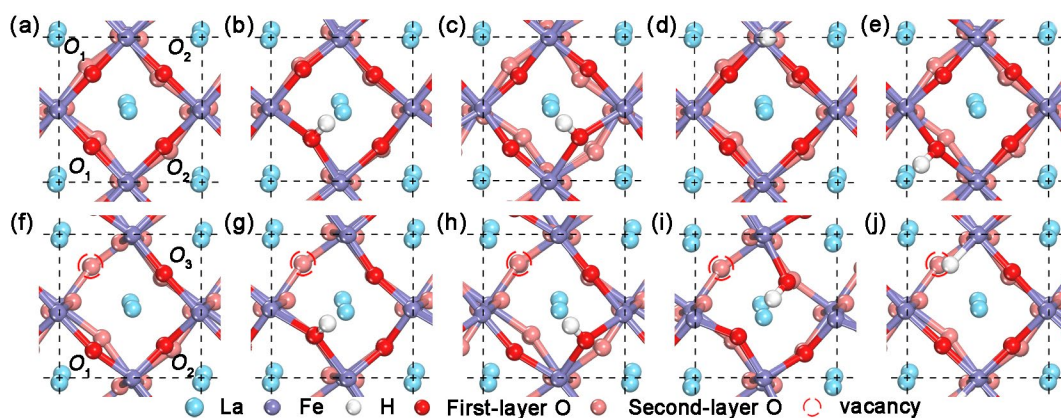
Fig. 1. Top views of optimized configurations of (a) defect-free $LaFeO_3$(001) surface, H adsorption at the (b) O_1, (c) O_2, and (d) Fe sites of the $LaFeO_3$(001) surface, (e) H adsorption at the O_1 sites with O-H bond orientated in an opposite direction to that in (b),

(f) defective LaFeO$_3$(001) surface with an oxygen atom removed, H adsorption at the (g) O_1, (h) O_2, and (i) O_3 sites, and (j) in the vacancy of the defective LaFeO$_3$(001) surface.

The optimized configurations of H adsorption at the three surface sites are shown in Fig. 1b-d. It should be noted that hydrogen could be bound to an O ion with the O-H bond orientated in two opposite directions (e.g., Fig. 1b vs. Fig. 1e). To explore the adsorption behavior of the defective LaMO$_3$ surfaces, an O ion is removed from the MO$_2$ termination, achieving an oxygen vacancy coverage of 1/4 ML. Since either O_1 or O_2 can be removed, two defective surfaces may result for each LaMO$_3$. Comparison of the surface oxygen vacancy formation energies indicates that the O_1 ion can be removed more readily than O_2 (The surface oxygen vacancy formation energies on the LaMO$_3$ surfaces are given in the Supporting Information). Hence, the defective LaMO$_3$(001) surface under consideration is based on the formation of oxygen vacancy at the O_1 site. Upon removal of an O_1 ion, the defective surface is left with three distinct oxygen sites, which have different chemical identities and thus denoted O_1, O_2, and O_3 (see Fig. 1f). The optimized configurations of H adsorption on the defective LaMO$_3$ surfaces are shown in Fig. 1g-j. One can see from the figure that H can be adsorbed not only on top of the three oxygen ions but also in the oxygen vacancy. In addition, on the defective LaCrO$_3$ surface H may be coordinated to the metal ion with the H-Cr bond oriented ~8 ° with respect to the z axis, whereas on the other two oxygen-deficient surfaces such an adsorption configuration cannot be attained.

To measure the strength of the interaction between H and the LaMO$_3$ surfaces, the adsorption energy (ΔE_{ads}) of hydrogen is defined as

$$\Delta E_{ads} = E_{surface-H} - E_{surface} - \frac{1}{2}E_{H_2} \qquad (1)$$

where $E_{surface-H}$ and $E_{surface}$ are the total energies of the surface with hydrogen adsorbed and the defect-free or defective LaMO$_3$ surface, respectively, and E_{H_2} is the total energy of an isolated hydrogen molecule. Under this definition, a negative value of the ΔE_{ads} shows the exothermic character of the adsorption process. The more negative the ΔE_{ads} value, the stronger is the interaction between hydrogen and the surface.

The adsorption energies at the different surface sites of the defect-free and defective LaMO$_3$(001) are shown in Fig. 2. From the figure, one can see that there is a slight difference in the adsorption behavior between the surfaces. On the three defect-free surfaces the adsorption of H at the O_1 site is energetically most favorable and the orientation of the O-H bond has a negligible effect on the strength of the interaction between the H and O ion. As H moves to the O_2 site and further to the M site, the binding strength becomes progressively weaker. On the defective LaMnO$_3$ and LaFeO$_3$ surfaces, although the O ions are still preferred by H atoms over the M site, the magnitude of the ΔE_{ads} at the O_1 site is lowered by 0.32 and 0.60 eV, respectively. By contrast, the H adsorption energy in the vacancy of the defective LaCrO$_3$(001) surface is 0.1 eV more negative than that at the O_1 sites; that is, the vacancy that is not preferred on the defective

11

LaMnO$_3$(001) and LaFeO$_3$(001) becomes most favorable for H adsorption. Moreover, on

the oxygen-deficient LaCrO$_3$(001) the H adsorption energies at the various surface sites lie

within a narrow range, and it is the only defective surface on which H can be stabilized at

the transition-metal site. On the other two defective surfaces, H would be optimized into

the adjacent vacancy even if it is initially positioned at the M site. These unique features

are expected to play a role in the hydrogen migration behavior on LaCrO$_3$(001).
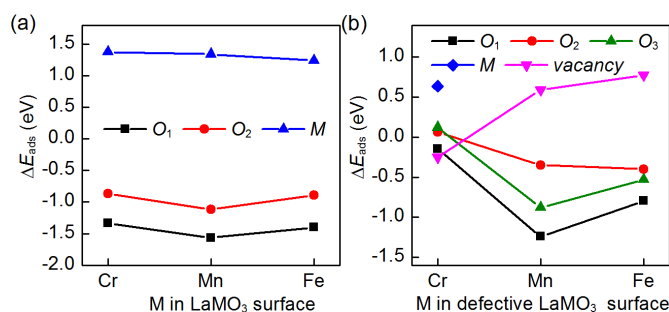
Fig. 2. Calculated ΔE_{ads} at different surface sites of (a) defect-free and (b) defective

LaMO$_3$(001) surfaces.

Upon H adsorption the three defect-free surfaces are distorted in much the same way and

to nearly the same extent. On LaFeO$_3$, for instance, the O ions are displaced out of the

surface by 0.024 and 0.032 Å at the O_1 and O_2 sites, respectively, with the O_1-H and O_2-H

bonds measured to be 0.984 and 0.985 Å, both of which are shorter than that in gaseous

OH (0.996 Å). Typically, the reduction in the O-H bond length can be reflected in the

increased O-H bond stretching frequency. Indeed, the calculated vibrational wavenumber

of the O_1-H bond, O_2-H bond, and free OH radical decreases from 3986 through 3801 and

eventually to 3722 cm^{-1}. In experiment, the same O-H bond contraction has been observed in molecular H_2O (0.958 Å bond length compared to 0.970 Å in free OH radicals).

It has long been recognized that the adsorption energy of a small species on a solid surface can be decomposed into the bonding energy that measures the strength of the direct interaction between them and the distortion energies of the adsorbate and substrate[40]. As a general rule, a bond shortens as it becomes stronger, and structure distortion is known to have a negative effect on the stability of the adsorbed species. Here the O-H bond length provides a measure of how strongly the O and H ions interact and the displacement of the O ion can be used to gauge the degree of the geometrical distortion of the substrate arising from H adsorption. Hence, the greater binding strength of H to the O_1 ion than to the O_2 ion can be explained by the shorter O-H bond length and less displacement of the surface O ion.

The relationship above holds true on the other two defect-free surfaces and is also valid on the defective surfaces. On the defective $LaFeO_3$ surface, although the O_2-H bond has a bond length (0.981 Å) very close to the O_1-H bond (0.982 Å) and is much shorter than the O_3-H bond (0.995 Å), the H adsorption energy at the O_2 site is significantly less negative than that at the O_1 site and even slightly less negative than that at the O_3 site, as can be seen in Fig. 2b. Detailed structural analysis indicates that the O_2 ion is displaced much more dramatically (0.070 Å) than the O_1 and O_3 ions (0.025 and 0.017 Å, respectively), which is largely responsible for the observed trend. As an another example, the O_2-H bond length (0.999 Å) on the defective $LaMnO_3$ surface compares closely to that of the O_3-H bond

(0.998 Å), but the adsorption energy at the O_2 site is much less negative than that at the O_3 site, which can also be attributed to the greater O_2 displacement (0.028 Å vs. 0.023 Å). The structural information including the O-H bond lengths and the displacements of surface O ions is given in the Supporting Information.
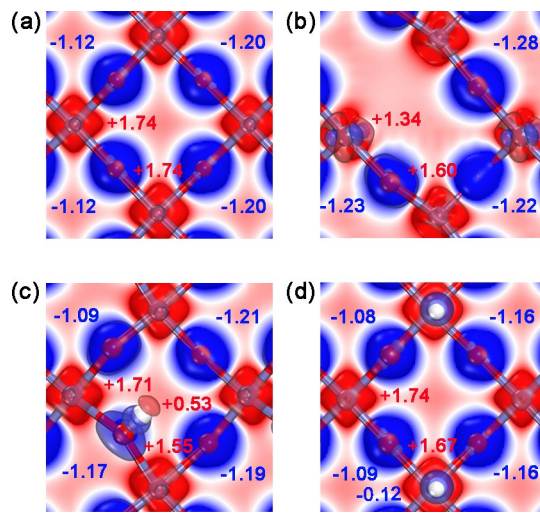

Fig. 3. Calculated effective Bader charges on atoms on (a) defect-free LaFeO$_3$ surface, (b) defective LaFeO$_3$ surface, (c) defect-free LaFeO$_3$ surface with an H atom adsorbed at the O_1 site, and (d) defect-free LaFeO$_3$ surface with an H atom adsorbed at the Fe site.

   To examine more closely the nature of the chemical bonds on the perovskite surfaces, the Bader charge analysis, which is based on the concept of a gradient vector path, was performed to keep track of the charge redistribution upon adsorption of an H atom. As indicated in Fig. 3a and 3b, the effective Bader charges on the O and Fe ions on the defective surface are more negative and less positive, respectively, than those on the defect-free surface, implying the electrons left behind upon removal of an oxygen atom

would delocalize over the whole outermost layer of the surface[41]. Thus, the increased electron density on the remaining O ions would limit their ability to withdraw electrons from H, which in turn weakens the O-H bond. Interestingly, as can be seen in Fig. 3c and 3d, hydrogen, which carries positive charges when bound to the O site, gains a certain number of electrons from surface O ions and becomes negatively charged when adsorbed at the Fe site. The more negative H adsorption energy at the O_l site than that at the Fe site can therefore be ascribed to the stronger attractive interaction between the O_l anion and the positively charged H. Moreover, the adsorbed H at the O_l site also interacts weakly with its neighboring surface oxygen ions via hydrogen bonding [the interatomic distance between them falls within the typical range over which intermolecular forces function (e.g., 2.20 - 3.20 Å on $LaFeO_3$)], which is absent when H sits on the Fe cation.

The Grotthuss mechanism for hydrogen migration on $LaMO_3$ surfaces. As stated in the Introduction, it was well agreed that the hydrogen migration in the bulk of transition-metal oxides follows the Grotthuss mechanism. Unlike in bulk perovskite where the M cation is octahedrally coordinated to oxygen, an enhanced electron occupancy of the out-of-plane orbitals arises on the surface, owing to the absence of apical oxygen coordination[42]. To gain insight into the mechanism for hydrogen migration on the $LaMO_3$ surfaces, the CI-NEB method was used to find the MEP for hydrogen surface transport. Considering the symmetry of the surfaces, there exist three possible elementary steps for hydrogen hopping between neighboring oxygen ions (steps a-c) and two possible elementary steps for O-H bond reorientation (steps d and e), as shown in Fig. 4a. The possibility of H

hopping from oxygen anions to metal cations is disregarded because such a process has a definitely high energy barrier given the H adsorption energy difference (over 2 eV) at these two sites.
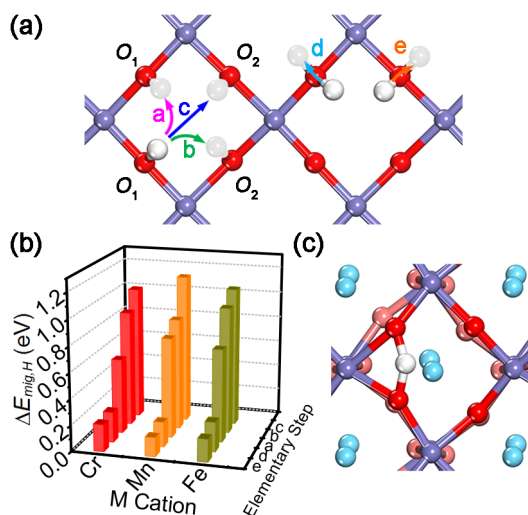
Fig. 4. (a) Top view of hydrogen migration elementary steps on the defect-free LaMO$_3$ surfaces; (b) calculated energy barriers for hydrogen migration elementary steps; and (c) geometry of the transition state for step a.

The calculated energy barriers for all the elementary steps on the three defect-free surfaces are presented in Fig. 4b. In particular, the hopping barriers vary from 0.5 eV to 1.2 eV, and step a is kinetically most favorable, regardless of the identity of the M cation. During the course of this step, the hydrogen hopping proceeds with O-H bond breaking initially at one O_1 site, followed by O-H bond formation at an adjacent O_1 site. In the transition state (see Fig. 4c), the hopping H is bonded simultaneously to the two O_1 ions at nearly the same interatomic distance and the O-H-O bond angle deviates from 180 ° due to

16

the Coulomb repulsion between the H^+ ion and the highly positively charged M cation. In order to promote hydrogen hopping, the two oxygen ions move toward each other to reduce the interionic distance, though the O-H bond is still significantly stretched and measured to be 1.2 - 1.3 Å. As for the O-H bond reorientation, the O-H bond in the transition state is aligned nearly perpendicular to the surface. The calculated barriers are in the range 0.1 - 0.3 eV, much lower than those for the hopping of H^+ ions, which has been verified experimentally in bulk perovskite[10-11]. For instance, the activation energy for the hydroxyl reorientation in a mixed perovskite, $Ba[Ca_{(1+x)/3}Nb_{(2-x)/3}]O_{3-x/2}$, is only about 0.10 eV, as determined by Quasi-elastic neutron scattering[10].

Long-range hydrogen transport is of crucial importance for many heterogeneous reactions, in which high catalytic performance cannot be attained unless hydrogen may "dance" freely on the surface. Taking the H adsorption at the energetically most favorable O_1 site as the starting and ending points, we find the hydrogen hopping and hydroxyl reorientation elementary steps can be combined into three diffusion pathways, as shown schematically in Fig. 5a. PATH(I) is essentially the hopping between the O_1 and O_2 site, consisting of steps b, d, and e that are connected in series and along the [100] axis. Similarly, PATH(II) and PATH(III) are extended along the [010] axis and the diagonal of the plane, respectively. As an example, the MEPs for the three diffusion pathways on $LaFeO_3$ are presented in Fig. 5b. The calculations reveal that on the defect-free surface hydrogen migrates preferentially along the [010] axis, during which the O-H bond is reoriented at the O_1 site for the hopping to proceed by the Grotthuss mechanism. From the energy profiles,

it follows that the rate for the overall process is determined by the hydrogen hopping rather than by the hydroxyl reorientation, as has already been observed for the hydrogen transport in bulk perovskite[11]. On the defect-free $LaCrO_3$ and $LaMnO_3$ surfaces, PATH(II) is also found to be the kinetically most favorable pathway and the energy barriers are calculated to be 0.58 and 0.77 eV, respectively.
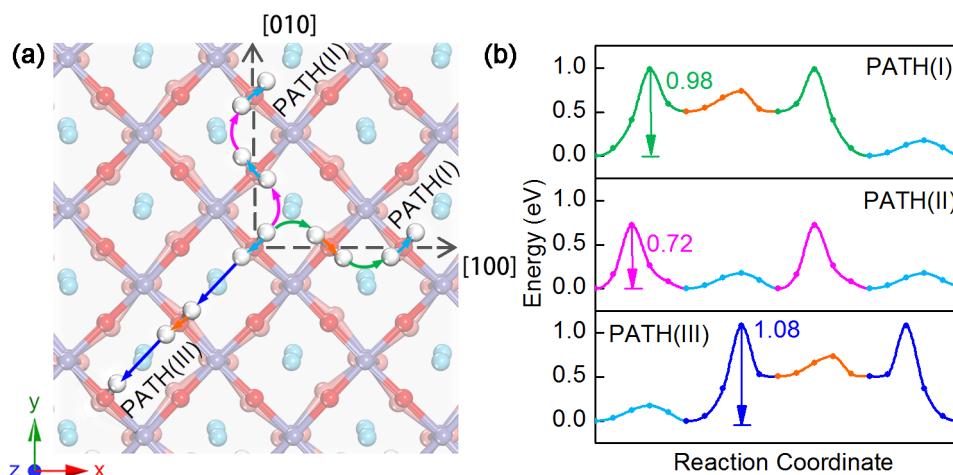
Fig. 5. (a) Illustration of the three hydrogen diffusion pathways on the defect-free $LaMO_3$ surfaces; (b) MEPs for the three hydrogen diffusion pathways on the defect-free $LaFeO_3$ surfaces.

The "vehicle" mechanism for hydrogen migration on defective $LaMO_3$ surfaces. It is well known that defects on the surface of perovskites often determine how they function and react, among which oxygen vacancies are perhaps most frequently encountered. The ability of perovskites to store and release oxygen as oxygen buffer or to promote the activity and dispersion of supported metal clusters can be traced to the presence of surface O vacancies. On the other hand, the removal of surface oxygen atoms would dramatically

increase the complexity in the hydrogen surface transport behavior. Apart from the

Grotthuss mechanism, an alternative way for hydrogen to migrate is to hop together with

the underlying oxygen ion as a whole, i.e., by the "vehicle" mechanism.
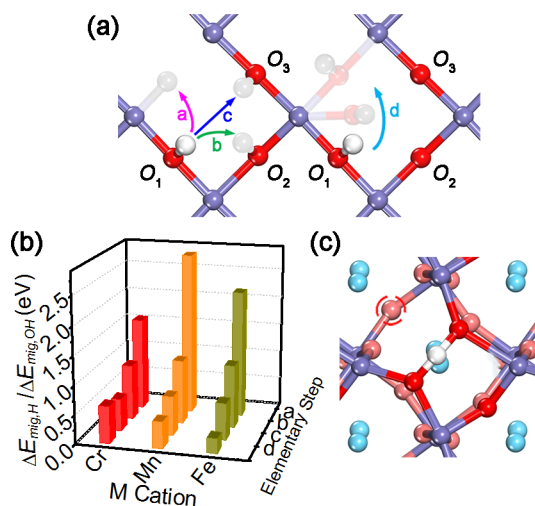
Fig. 6. (a) Illustration of hydrogen and hydroxyl migration elementary steps on the

defective $LaMO_3$ surface and (b) calculated energy barriers for hydrogen and hydroxyl

migration elementary steps; (c) geometry of the transition state for step c.

For ease to compare, here we also take the H adsorption at the O_1 site as the initial state

for hydrogen migration on the defective surfaces. Like on the defect-free counterparts,

three possible elementary steps are identified, as shown in Fig. 6a. In step a, H hops

between the O_1 and vacancy site, and steps b and c refer to the hopping of H between two

neighboring oxygen ions. In addition, the hopping of hydroxyl ions via oxygen vacancy is

considered and illustrated in Fig. 6a as well. The minimum energy required to surmount

the energy barriers for the hydrogen and hydroxyl migration elementary steps are shown in Fig. 6b.

Our calculated results indicate that step c is kinetically preferred over the other two hydrogen hopping steps. It is worth noting that the O-H bond reorientation is likely to be a barrier-free process at the O_1 site and, at the O_3 site, the corresponding energy barriers, although nonzero, are negligibly low (about 0.2 eV) compared to the hydrogen hopping barriers. In the transition state for step c (see Fig. 6c), the hopping H is coordinated to the two O ions in nearly a straight line, with a closer distance to the O_1 site. Further comparison of the lowest-energy barriers for the hydrogen and hydroxyl migration reveals that the hydrogen transport may follow different mechanisms on different defective surfaces. On the defective $LaMn_3(001)$ and $LaFeO_3(001)$, the energy barrier for step d is markedly lower than that for step c and, consequently, hydrogen prefers to migrate together with the underlying O by the "vehicle" mechanism. On the $LaCrO_3$ surface, however, the opposite is true, meaning that the Grotthuss mechanism would prevail once hydrogen is captured by the O ions during the reaction.

Considering that the hydroxyl migration barrier is lower than that for the hydrogen migration on the defect-free $LaMnO_3(001)$ and $LaFeO_3(001)$, it can be deduced that the hydrogen mobility would be promoted by the formation of surface oxygen vacancies. On the $LaCrO_3$ surface, hydrogen favors the vacancy site, from which the migration of hydrogen needs to overcome a particularly high energy barrier (1.72 eV, which is, in essence, the energy barrier for the reverse of step a), and thus tends to be "trapped"

therein; that is, the presence of surface vacancies has a negative effect on the hydrogen transport in this case.

The factor determining the energy barrier for hydrogen and hydroxyl migration on LaMO₃ surfaces. In early studies, many physical properties have been proposed to explain the trend in the hydrogen transport kinetics in bulk oxide. By conducting complex impedance analysis over a wide range of frequencies, Scherban et al.[43] suggested that the activation energy for proton transport in Fe-doped $KTaO_3$, Yb-doped $SrCeO_3$ and $BaCeO_3$ decreases with increasing the interatomic distance between oxygen ions. More recently, Kreuer et al.[11] claimed that a "soft" array of oxygen is highly required for rapid proton transfer and the fluctuation of the oxygen separation coordinate would decrease the effective transfer barrier and thus increase the proton transfer rate. In this work, however, the interatomic distance between O ions is found to bear no direct relation to the calculated hydrogen migration barrier (see Fig. S2). Through a combined experimental and theoretical study, Karlsson et al.[13] pointed out that the proton mobility depends strongly upon the degree of hydrogen bonding between proton and its adjacent oxygen, in the sense that a stronger hydrogen bonding would increase the proton transfer rate but simultaneously suppress the reorientation of the O-H bond that requires the breaking of the hydrogen bonds. Hence, despite the many studies, there is not uniform agreement on the major factor that determines the energy barrier for hydrogen and hydroxyl migration on the perovskite surfaces.
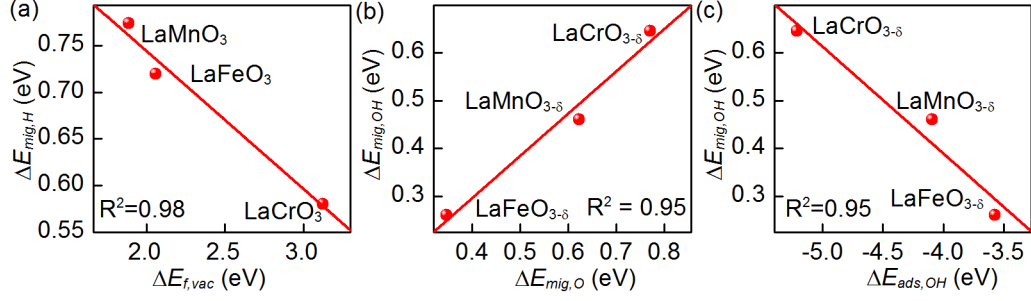
Fig. 7. (a) Plot of energy barrier for hydrogen migration ($\Delta E_{mig,H}$) on defect-free surfaces against formation energy of surface oxygen vacancy ($\Delta E_{f,vac}$), (b) plot of hydroxyl migration barrier ($\Delta E_{mig,OH}$) against oxygen migration barrier ($\Delta E_{mig,O}$) on defective surfaces, and (c) plot of hydroxyl migration barrier against adsorption energy of OH on defective surfaces ($\Delta E_{ads,OH}$).

In the present work, both structural and energetic properties have been used to correlate data on the calculated energy barriers. It is found that the hydrogen migration barrier on the defect-free surfaces scales linearly with the surface oxygen formation energy, which is defined as the energy required to remove an oxygen atom from the oxide surface. Although the calculated surface oxygen vacancy formation energies are less positive than their respective counterparts in the bulk (5.41, 3.96, and 4.73 eV for $LaCrO_3$, $LaMnO_3$, and $LaFeO_3$, respectively[44]), the exceptionally high vacancy formation energy on $LaFeO_3$ is still observed, which can be explained by the preference for maximum electron exchange stabilization in Fe^{3+} ions[45]. In addition, the negative slope of the straight line means that the more strongly the attraction between surface O and the remaining oxide lattice, the less

tightly is the H bound to the O site, and hence the more readily can the hydrogen hop on the oxide surface.
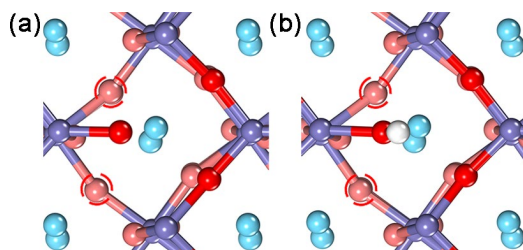
Fig. 8. Geometries of the transition states for (a) oxygen and (b) hydroxyl hopping on the defective surfaces.

On the defective $LaMnO_3$ and $LaFeO_3$ surfaces, the hydrogen transport follows the "vehicle" mechanism, moving together with the underlying O ion. Fig. 8 shows the transition states for the oxygen and hydroxyl migration on the defective $LaFeO_3(001)$. One can see that upon hopping of the two species the oxide surfaces are distorted in exactly the same way. It is therefore not surprising to learn that the energy barrier for the hydroxyl migration increases linearly with that for the oxygen migration (see Fig. 8b). Moreover, the slope of the straight line is less than unity, which indicates that oxygen may hop more readily by carrying a hydrogen. The underlying reason is due to the weakening of the M-O bond, as is reflected in the elongated M-O bond length (The corresponding data are included in the Supporting Information).

Interestingly, the energy barriers for hydroxyl and oxygen migration both decrease as we move from $LaCrO_3$ through $LaMnO_3$ and eventually to $LaFeO_3$, which cannot be

rationalized in terms of the vacancy formation energy on the defect-free surfaces. Given the fact that both removal of an oxygen atom from the perovskite surface and adsorption of H on an O ion would contribute to the reduction of the nearby transition-metal cation to that having a formal oxidation number lower than +3 (see Fig. 3), the further electron transfer that occurs during the course of the hopping of OH would give rise to the stepwise occupation of the 4s orbital of the transition metal. As a consequence, the total energy of the system would not be lowered by the desire to maximize the exchange stabilization in the 3d orbitals. Based on this information, we then plot the hydroxyl migration barrier against the energy change associated with the removal of the OH radical from the oxygen-deficient LaMO$_3$ surface, and a good linear scaling relation is established (see Fig. 7c), which means that a weakened M-O bond strength would give rise to a more facile hydroxyl transport.

   Having obtained these linear scaling relations, we are now in a position to understand the major factor responsible for the change in the preferred migration mechanism on going from the defective LaCrO$_3$ to LaMnO$_3$ and LaFeO$_3$. It can be seen that the hydrogen and hydroxyl migration barriers generally decrease and increase with increasing the strength of ionic bonding in perovskites. When the M-O bond strength is great, the energy barrier for hydrogen migration is lower, as is observed on all the defect-free LaMO$_3$ surfaces and the defective LaCrO$_3$. When the ionic bonding is weakened to a certain extent, however, the hydroxyl migration becomes kinetically preferred, which is the reason why the "vehicle"

mechanism dominates on the defective LaMnO$_3$(001) and LaFeO$_3$(001) whereas the Grotthuss mechanism prevail on the defective LaCrO$_3$(001).

CONCLUSIONS

In this work, periodic DFT+U calculations have been carried out to study the hydrogen transport behaviors on the defect-free and defective LaMO$_3$ surfaces (M = Cr, Mn, and Fe). Our calculated results indicate that H atoms would be preferentially adsorbed at the O sites on all the surfaces other than the defective LaCrO$_3$(001), where the occupation of vacancies is energetically most favorable. The resultant O-H bonds would be weakened when oxygen vacancies are formed in their immediate vicinity because the electrons left behind upon removal of an oxygen atom would delocalize over the whole outermost layer of the oxide surface and the increased electron density on the remaining O ions would limit their ability to withdraw electrons from H. In addition, it turns out that the hydrogen migration may follow different mechanisms on different surfaces. On the defect-free LaMO$_3$(001) hydrogen prefers to migrate along the [010] axis, during which the O-H bond is reoriented at the oxygen site for the hopping to proceed by the Grotthuss mechanism. When surface oxygen vacancies are present, the hydroxyl migration barrier on LaMnO$_3$ and LaFeO$_3$ is found to be markedly lower than that for hydrogen migration and the "vehicle" mechanism should dominate. On the defective LaCrO$_3$(001), however, the opposite is true, meaning that the Grotthuss mechanism would prevail once hydrogen is captured by the O ions during the reaction. The linear scaling relations established show that the hydrogen and hydroxyl migration barriers generally decrease and increase, respectively, with

increasing the strength of ionic bonding in perovskites, which provides a rational interpretation of the change in the preferred hydrogen surface migration mechanism.

ASSOCIATED CONTENT

Supporting Information. Convergence of H adsorption energy with respect to cell size. Convergence of H adsorption energy with respect to slab thickness. Surface oxygen vacancy formation energy. Displacements of O ions and the O-H bond lengths on H-adsorbed surfaces. M-O bond lengths on defective perovskite surfaces. Relationship between the hydrogen migration barrier and d_{O-O}.

ACKNOWLEDGEMENTS

REFERENCES

1.   Avila-Paredes, H. J.; Zhao, J.; Wang, S.; Pietrowski, M.; De Souza, R. A.; Reinholdt, A.; Munir, Z. A.; Martin, M.; Kim, S., Protonic conductivity of nano-structured yttria-stabilized zirconia: dependence on grain size. *J Mater Chem* **2010,** *20* (5), 990-994.
2.   Miyoshi, S.; Akao, Y.; Kuwata, N.; Kawamura, J.; Oyama, Y.; Yagi, T.; Yamaguchi, S., Water uptake and conduction property of nano-grained yttria-doped zirconia fabricated by ultra-high pressure compaction at room temperature. *Solid State Ionics* **2012,** *207*, 21-28.
3.   Manabe, R.; Okada, S.; Inagaki, R.; Oshima, K.; Ogo, S.; Sekine, Y., Surface Protonics Promotes Catalysis. *Sci Rep* **2016,** *6*, 38007.

4. Zheng, Q.; Tan, S.; Feng, H.; Cui, X.; Zhao, J.; Wang, B., Dynamic Equilibrium of Reversible Reactions and Migration of Hydrogen Atoms Mediated by Diffusive Methanol on Rutile TiO2 (110)-(1 × 1) Surface. *J Phys Chem C* **2016,** *120* (14), 7728-7735.

5. Kim, S.; Avila-Paredes, H. J.; Wang, S.; Chen, C. T.; De Souza, R. A.; Martin, M.; Munir, Z. A., On the conduction pathway for protons in nanocrystalline yttria-stabilized zirconia. *Phys Chem Chem Phys* **2009,** *11* (17), 3035-3038.

6. Zhang, Z.; Du, Y.; Petrik, N. G.; Kimmel, G. A.; Lyubinetsky, I.; Dohnálek, Z., Water as a Catalyst: Imaging Reactions of O2 with Partially and Fully Hydroxylated TiO2(110) Surfaces. *J Phys Chem C* **2009,** *113* (5), 1908-1916.

7. Pang, C. L.; Lindsay, R.; Thornton, G., Chemical reactions on rutile TiO2(110). *Chem Soc Rev* **2008,** *37* (10), 2328.

8. Kreuer, K. D., Proton Conductivity: Materials and Applications. *Chem Mater* **1996,** *8* (3), 610-641.

9. Kreuer, K. D., On the complexity of proton conduction phenomena. *Solid State Ionics* **2000,** *136-137*, 149-160.

10. Pionke, M.; Mono, T.; Schweika, W.; Springer, T.; Schober, H., Investigation of the hydrogen mobility in a mixed perovskite: Ba[Ca(1+x)/3Nb(2−x)/3]O3−x/2 by quasielastic neutron scattering. *Solid State Ionics* **1997,** *97* (1), 497-504.

11. Kreuer, K. D.; Fuchs, A.; Maier, J., HD isotope effect of proton conductivity and proton conduction mechanism in oxides. *Solid State Ionics* **1995,** *77*, 157-162.

12. Matzke, T.; Stimming, U.; Karmonik, C.; Soetratmo, M.; Hempelmann, R.; Güthoff, F., Quasielastic thermal neutron scattering experiment on the proton conductor SrCe0.95Yb0.05H0.02O2.985. *Solid State Ionics* **1996,** *86-88*, 621-628.

13. Karlsson, M.; Björketun, M. E.; Sundell, P. G.; Matic, A.; Wahnström, G.; Engberg, D.; Börjesson, L.; Ahmed, I.; Eriksson, S.; Berastegui, P., Vibrational properties of protons in hydrated BaInxZr1−xO3−x∕2. *Phys Rev B* **2005,** *72* (9), 094303.

14. Norby, T., Proton conduction in oxides. *Solid State Ionics* **1990,** *40-41*, 857-862.

15. Tao, Z.; Yan, L.; Qiao, J.; Wang, B.; Zhang, L.; Zhang, J., A review of advanced proton-conducting materials for hydrogen separation. *Prog Mater Sci* **2015,** *74*, 1-50.

16. Nowick, A. S.; Du, Y., High-temperature protonic conductors with perovskite-related structures. *Solid State Ionics* **1995,** *77*, 137-146.

17. Kim, J. S.; Kim, Y. C., Proton conduction across and along BaO− and ZrO2−terminated (001) BaZrO3 surfaces using density functional theory. *Solid State Ionics* **2017,** *306*, 137-141.

18. Kim, J. S.; Yang, J. H.; Kim, B. K.; Kim, Y. C., Proton conduction at BaO-terminated (001) BaZrO3 surface using density functional theory. *Solid State Ionics* **2015,** *275*, 19-22.

19. Kowalski, P. M.; Meyer, B.; Marx, D., Composition, structure, and stability of the rutile TiO2(110) surface: Oxygen depletion, hydroxylation, hydrogen migration, and water adsorption. *Phys Rev B* **2009,** *79* (11), 115410.

20. Yin, X. L.; Calatayud, M.; Qiu, H.; Wang, Y.; Birkner, A.; Minot, C.; Wöll, C., Diffusion versus Desorption: Complex Behavior of H Atoms on an Oxide Surface. *Chemphyschem* **2008,** *9* (2), 253-256.

21. Pena, M. A.; Fierro, J. L. G., Chemical structures and performance of perovskite oxides. *Chem Rev* **2001,** *101* (7), 1981-2017.

22. Royer, S.; Duprez, D.; Can, F.; Courtois, X.; Batiot-Dupeyrat, C.; Laassiri, S.; Alamdari, H., Perovskites as Substitutes of Noble Metals for Heterogeneous Catalysis: Dream or Reality. *Chem Rev* **2014,** *114* (20), 10292-10368.

23. Kresse, G.; Hafner, J., Ab initio molecular dynamics for open-shell transition metals. *Phys Rev B* **1993,** *48* (17), 13115.

24. Kresse, G.; Furthmüller, J., Efficient iterative schemes for ab initio total-energy calculations using a plane-wave basis set. *Phys Rev B* **1996,** *54* (16), 11169-11186.

25. Kresse, G.; Furthmüller, J., Efficiency of ab-initio total energy calculations for metals and semiconductors using a plane-wave basis set. *Comp Mater Sci* **1996,** *6* (1), 15-50.

26. Wellendorff, J.; Lundgaard, K. T.; Møgelhøj, A.; Petzold, V.; Landis, D. D.; Nørskov, J. K.; Bligaard, T.; Jacobsen, K. W., Density functionals for surface science: Exchange-correlation model development with Bayesian error estimation. *Phys Rev B* **2012,** *85* (23), 235149.

27. Kresse, G.; Joubert, D., From ultrasoft pseudopotentials to the projector augmented-wave method. *Phys Rev B* **1999,** *59* (3), 1758-1775.

28. Cohen, A. J.; Mori-Sánchez, P.; Yang, W., Insights into Current Limitations of Density Functional Theory. *Science* **2008,** *321* (5890), 792.

29. Anisimov, V. I.; Aryasetiawan, F.; Lichtenstein, A. I., First-principles calculations of the electronic structure and spectra of strongly correlated systems: the LDA + U method. *J. Phys.: Condens. Matter* **1997,** *9* (4), 767-808.

30. Anisimov, V. I.; Zaanen, J.; Andersen, O. K., Band theory and Mott insulators: Hubbard U instead of Stoner I. *Phys Rev B* **1991,** *44* (3), 943-954.

31. Dudarev, S. L.; Botton, G. A.; Savrasov, S. Y.; Humphreys, C. J.; Sutton, A. P., Electron-energy-loss spectra and the structural stability of nickel oxide: An LSDA+U study. *Phys Rev B* **1998,** *57* (3), 1505-1509.

32. Li, Y.; Zheng, Y. S.; Zhu, Y. A.; Sui, Z. J.; Zhou, X. G.; Chen, D.; Yuan, W. K., BEEF-vdW+U method applied to perovskites: thermodynamic, structural, electronic, and magnetic properties. *J. Phys.: Condens. Matter* **2019,** *31* (14), 145901.

33. Wang, L.; Maxisch, T.; Ceder, G., Oxidation energies of transition metal oxides within the GGA+U framework. *Phys Rev B* **2006,** *73* (19), 195107.

34. Jain, A.; Hautier, G.; Ong, S. P.; Moore, C. J.; Fischer, C. C.; Persson, K. A.; Ceder, G., Formation enthalpies by mixing GGA and GGA +U calculations. *Phys Rev B* **2011,** *84* (4), 045115.

35. Zeng, Z.; Chan, M. K. Y.; Zhao, Z.-J.; Kubal, J.; Fan, D.; Greeley, J., Towards First Principles-Based Prediction of Highly Accurate Electrochemical Pourbaix Diagrams. *J Phys Chem C* **2015,** *119* (32), 18177-18187.

36. Goodenough, J. B., Localized versus Collective d Electrons and Néel Temperatures in Perovskite and Perovskite-Related Structures. *Phys. Rev.* **1967,** *164* (2), 785-789.

37. Monkhorst, H. J.; Pack, J. D., Special points for Brillouin-zone integrations. *Phys Rev B* **1976,** *13* (12), 5188-5192.

38. Henkelman, G.; Jónsson, H., Improved tangent estimate in the nudged elastic band method for finding minimum energy paths and saddle points. *J Chem Phys* **2000,** *113* (22), 9978-9985.

39. Henkelman, G.; Uberuaga, B. P.; Jónsson, H., A climbing image nudged elastic band method for finding saddle points and minimum energy paths. *J Chem Phys* **2000,** *113* (22), 9901-9904.

40. Fan, C.; Zhu, Y. A.; Xu, Y.; Zhou, Y.; Zhou, X. G.; Chen, D., Origin of synergistic effect over Ni-based bimetallic surfaces: A density functional theory study. *J Chem Phys* **2012,** *137* (1), 014703.

41. Li, Q.; Deng, Y. X.; Zhu, Y. A.; Li, Y.; Sui, Z. J.; Chen, D.; Yuan, W. K., Structural stability of Lanthanum-based oxygen-deficient perovskites in redox catalysis: A density functional theory study. *Catal Today* **2018**.

42. Pesquera, D.; Herranz, G.; Barla, A.; Pellegrin, E.; Bondino, F.; Magnano, E.; Sánchez, F.; Fontcuberta, J., Surface symmetry-breaking and strain effects on orbital occupancy in transition metal perovskite epitaxial films. *Nat Commun* **2012,** *3* (1), 1189.

43. Scherban, T.; Lee, W. K.; Nowick, A. S., Bulk protonic conduction in Yb-doped SrCeO3 and BaCeO3. *Solid State Ionics* **1988,** *28-30*, 585-588.

44. Zheng, Y. S.; Zhang, M.; Li, Q.; Zhu, Y. A.; Sui, Z. J.; Chen, D.; Zhou, X. G., Electronic Origin of Oxygen Transport Behavior in La-Based Perovskites: A Density Functional Theory Study. *J Phys Chem C* **2019,** *123* (1), 275-290.

45. Pavone, M.; Ritzmann, A. M.; Carter, E. A., Quantum-mechanics-based design principles for solid oxide fuel cell cathode materials. *Energy Environ Sci* **2011,** *4* (12), 4933-4937.
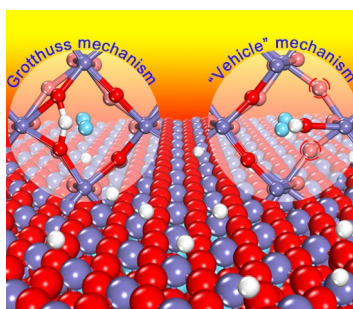
TOC Graphic

A change in the proton transport mechanism from the Grotthuss mechanism to the "vehicle" mechanism is observed on perovskite surfaces.